World Journal of Advanced Engineering Technology and Sciences
eISSN: 2582-8266
Cross Ref DOI: 10.30574/wjaets
Journal homepage: https://wjaets.com/

(RESEARCH ARTICLE)

Check for updates

Interaction between Electromagnetic (EM) wave and human head: Normal adult and elderly heads

Gasmelseed Akram *

College of Applied Medical Sciences, Qassim University, Saudi Arabia.

World Journal of Advanced Engineering Technology and Sciences, 2024, 13(01), 176–186

Publication history: Received on 27 July 2024; revised on 06 September 2024; accepted on 09 September 2024

Article DOI: https://doi.org/10.30574/wjaets.2024.13.1.0391

Abstract

In recent years, there has been an increasing public concern about the health implications of electromagnetic (EM) wave exposure with the use of mobile telephones. In this paper, we have evaluated the EM absorption in the human head at GSM 900 MHz (Global System for Mobile telecommunications) and DCS 1800 MHz (Digital Cellular System) radiation. Two models for human head were considered. The first model was normal adult head whereas the second model was normal elderly head. First, a stratified structure of the human head is modeled. Next, a two-dimensional (2-D) cylindrical head model based on finite-difference time-domain (FDTD) method is investigated. Our previous described 2-D FDTD code based on LabVIEW has been utilized. Much attention has been paid to the induced specific absorption rate (SAR) in elderly human head.

Keywords: Stratified Structure; Concentric Cylindrical Model; Finite Difference Time Domain (FDTD); Specific Absorption Rate (SAR); LabVIEW Programming Language

1. Introduction

There have been numerous reports on the effects of electromagnetic (EM) radiation on the human head when exposed to an incident plane wave [1-4]. When the radio frequency radiation is emitted from a mobile phone, held next to the human head, a portion is radiated away into the surrounding environment, and another portion is scattered and absorbed by tissues in the head and neck region of the body. Safety limits for EM exposure have been proposed by national and international organizations [5][6].

In the frequency 900 and 1800 MHz, the primary dosimetric parameter for the evaluation of the exposure is the specific absorption rate (SAR). SAR is defined as the power absorbed by the unit of mass of tissue (watts/kilogram). Much attention has been paid to the induced SAR in the human head for exposure to EM waves.

In this paper, the authors focused on the EM wave absorption in the human head at 900 MHz and 1800 MHz radiation. Two models for human head were considered. The first model was normal adult head, whereas the second model was normal elderly head, clarifying the effect of aging-related variations of the normal human head on the induced SAR.

It has been shown that with aging there is cortical atrophy (shrinkage) [7] [8]. These tend to be greater after the age of 60, and correlate with age cognitive impairment. This age-related atrophy also coincides with the weight loss and expansion of the ventricular volume [9] in the aged brain.

The investigation presented in this paper is divided into two parts. First, a stratified structure of the human head [10] is modeled in order to have some quantitative appreciation of the characteristic of the interaction between the EM

* Corresponding author: Gasmelseed Akram

waves and human head. Next, a two-dimensional (2-D) cylindrical head model based on finite-difference time-domain (FDTD) method [11] [12] is investigated.

As computing hardware became faster and more widely available, the FDTD method found numerous applications in electromagnetic radiation, scattering, and coupling. Stimulated by these successes, various researchers developed enhancements to the original technique that greatly extended its range of applicability. LabVIEW – Laboratory Virtual Instrument Engineering Workbench – is a National Instruments program development application [13] [14], similar to various C or FORTRAN development systems. However, LabVIEW is different from those applications in one important respect. Other programming systems use text-based languages to create lines of code, while LabVIEW uses a graphical programming language G, to create programs in block diagram form. The LabVIEW program codes provide a graphical user interface (GUI) to the model that makes it easy to observe and modify the behavior of each element of the model. In addition, the codes are relatively easy to understand and can be easily modified for the user's specific purpose.

2. Methodology and Calculations

2.1. Stratified Structure of human head

In our first approach, we attempt to understand how the RF wave is reflected from the dielectric layers in the model. In this case, the human head is regarded as a stratified medium composed of isotropic homogeneous lossy dielectric layers of planar geometry. Fig. 1 shows the geometry of the problem. A plane wave is incident upon the medium and traveling in the positive *+z* direction with the electric field vector linearly polarized along the *x*-axis.

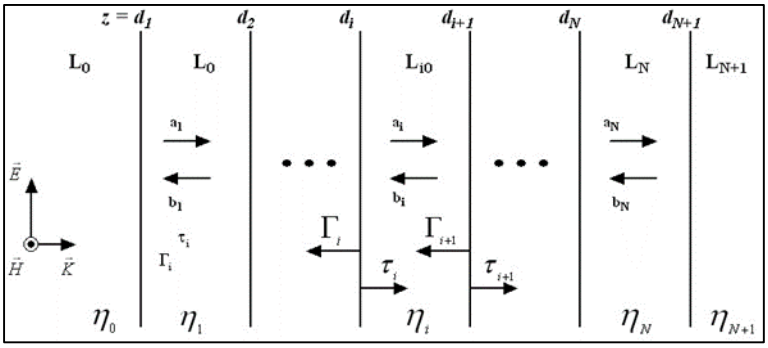

Figure 1 General structure o arbitrary stratified medium

The incident wave is assumed to have harmonic time variation $e^{j\omega t}$. There are *N+2* layers L_0, L_1,..., L_{N+1}, and *N+1* interfaces (d_1,...,d_{N+1}). The *ith* layer indicated by L_i has permittivity ε_i (F/m), permeability μ_i (H/m), and conductivity σ_i (S/m). Further, we denote the left-most layer (i.e. air) as L_0, while we denote the right-most layer by L_{N+1}. The electric (E_i) and magnetic (H_i) fields in the *ith* layer are given by

$$\overline{E}_i = \left(a_i e^{-jk_i z} + b_i e^{jk_i z}\right)\hat{x} \quad \text{..... (1)}$$

$$\overline{H}_i = \frac{\left(a_i e^{-jk_i z} - b_i e^{jk_i z}\right)}{\eta_i}\hat{y} \quad \text{..... (2)}$$

where $i = 0,1,...,N+1$. E_i and H_i are expressed in units of V/m and A/m, respectively. The constant a_i is the amplitude and phase of the incident wave in the *ith* layer; b_i is the amplitude and phase of reflected wave. k_i and η_i denotes the propagation constant and the intrinsic impedance of L_i respectively, and are given by

$$k_i^2 = \omega^2 \mu_i \varepsilon_i - j\omega\mu_i\sigma_i \quad \text{.....(3)}$$

$$\eta_i = \sqrt{\frac{\mu_i}{\varepsilon_i - j(\sigma_i/\omega)}} \quad \text{.....(4)}$$

The wave impedance is given by

$$Z_i = \eta_i \frac{\left(1+\Gamma_{i+1}e^{2jk_i d_i}\right)}{\left(1-\Gamma_{i+1}e^{2jk_i d_i}\right)} \quad \text{..... (5)}$$

At the interface $z = di$, the reflection coefficient Γ_i and the transmission coefficient τ_i is given by

$$\Gamma_i = \frac{\left(Z_i - \eta_{i-1}\right)}{\left(Z_i - \eta_{i-1}\right)} e^{-2jk_{i-1}d_i} \quad \text{..... (6)}$$

$$\tau_i = \frac{2Z_i}{Z_i + \eta_{i-1}} \frac{e^{j(k_i - k_{i-1})d_i}}{\left(1+\Gamma_{i+1}e^{2jk_i d_i}\right)} \quad \text{..... (7)}$$

Since $b_{N+1} = 0$, it follows that $\Gamma_{N+2} = 0$. Thus from (5), Z_{N+1} is equal to η_0, the intrinsic impedance of free space. By using equations (4), (6) and (7) we compute Γ_{N+1} and τ_{N+1}. We repeat the procedure by computing Z_N, Γ_N, τ_N and so on recursively, until Γ and τ have been evaluated at each interface. Then, we compute the complex constants using the following equations

$$\Gamma_i = b_{i-1}/a_{i-1} \quad \text{..... (6)}$$

$$\tau_i = a_i/a_{i-1} \quad \text{.....(7)}$$

Finally, we use equations (1) and (2) to calculate the electric and magnetic fields in L_i.

Once the induced electric field inside the stratified structure is known, the power density (W/m^3) absorbed along the *ith* layer from the sinusoidal field of the amplitude E_i is given by

$$P_i = \frac{\left|E_i\right|^2 \sigma_i}{2} \quad \text{.....(8)}$$

where σ_i is the conductivity of the *ith* layer (S/m). The local specific absorption rate (SAR), defined as the power absorbed by the unit mass of tissue, is given by

$$sar_i = P_i/\rho_i \quad \text{..... (9)}$$

where ρ_i is the tissue density (kg/m^3).

The squared magnitude $0 \le |\Gamma|^2 \le 1$ of the reflection coefficients is a direct measure of the ratio of reflected power to incident power, while $1-|\Gamma|^2$ is the proportion of incident wave power that is absorbed by the layered structure. Therefore, dips in $|\Gamma|$ indicate frequency ranges in which some of the incident wave power is absorbed. Even though $|\Gamma| \approx 1$implies that nearly all wave power is reflected away and power absorption is insignificant.

The model for the human head was taken from Functional Anatomy by Szentagothai Janos [15]. The human head is modeled by 8-layer stratified medium, as shown in Fig. 2, consisting of skin, fat, bone of skull, dura, subarachnoid cerebrospinal fluid (S-CSF), gray matter, white matter and cerebrospinal fluid (CSF).

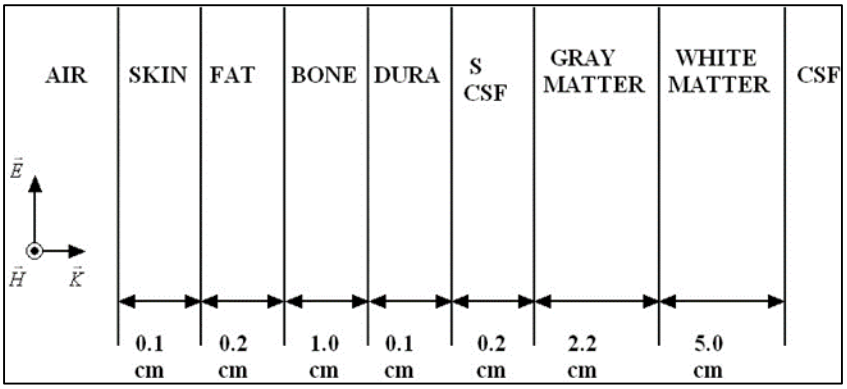

Figure 2 Stratified model of normal adult human head (N = 8)

The dielectric properties of tissues are evaluated by use of the four-term Cole-Cole equation

$$\varepsilon(\omega) = \varepsilon_{\infty} + \sum_{i=1}^{4} \frac{\Delta\varepsilon_i}{1+(-j\omega\tau_i)^{(1-\alpha_i)}} + j\frac{\sigma}{\omega\varepsilon_0} \quad \text{..... (10)}$$

where ε is the complex permittivity, ω = 2πf, and ε_0 is the permittivity of free space [16]. The permittivity and conductivity of tissues are given in Table I for excitation frequencies equal to 900 MHz and 1800 MHz (http://www.fcc.gov/fcc-bin/dielec.sh).

Thicknesses of skin, at, bone, dura and S-CSF layers were kept constant. The overall radius of the normal adult head is *9.75 cm*. For an aged head the thickness for gray and white matters reduced to *54.5%* and *60%* respectively, whereas thickness for CSF increased to *40%*.

Table 1 Thickness (d)[a] in cm, relative permittivity (ε_r) , conductivity (σ) in S/m and density (ρ) in Kg/m^3

Tissue	**d[1]**	**ε_r**		**σ**		**ρ**
		900	**1800**	**900**	**1800**	
Skin	0.1	41.4	38.9	0.867	1.185	1100
Fat	0.2	11.3	11.0	0.109	0.190	920
Bone	1.0	12.5	11.8	0.143	0.275	1850
Dura	0.05	44.4	42.9	0.961	1.320	1050
S – CSF	0.2	68.6	67.2	2.413	2.924	1060
Graymatter	2.2	52.7	50.1	0.942	1.391	1030
Whitematter	5.0	38.9	37.0	0.591	0.915	1030
CSF	2.0	68.6	67.2	2.413	2.924	1060

[1]Thickness of normal adult head

The electric field intensity E_i and SAR have been calculated in each layer of the structure for an incident power density of 1 mW/cm^2 at 900 MHz and 1800 MHz respectively (Fig. 3 and 4).

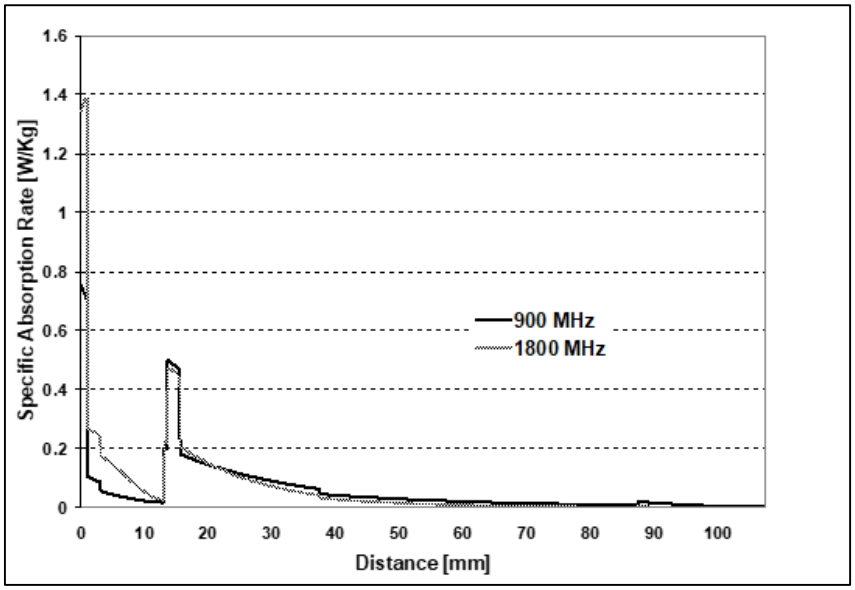

Figure 3 Local SAR distribution in normal adult head.

.Fig. 5 and 6 show the magnitude of reflection coefficients. It can be seen that, for the adult head model at both frequencies most of the energy is mainly reflected by the skin (-10.6 dB) and the fat (-17.6 dB) layers. On the other hand, for the elderly head model the reflectivity decrease for most of the head tissues.

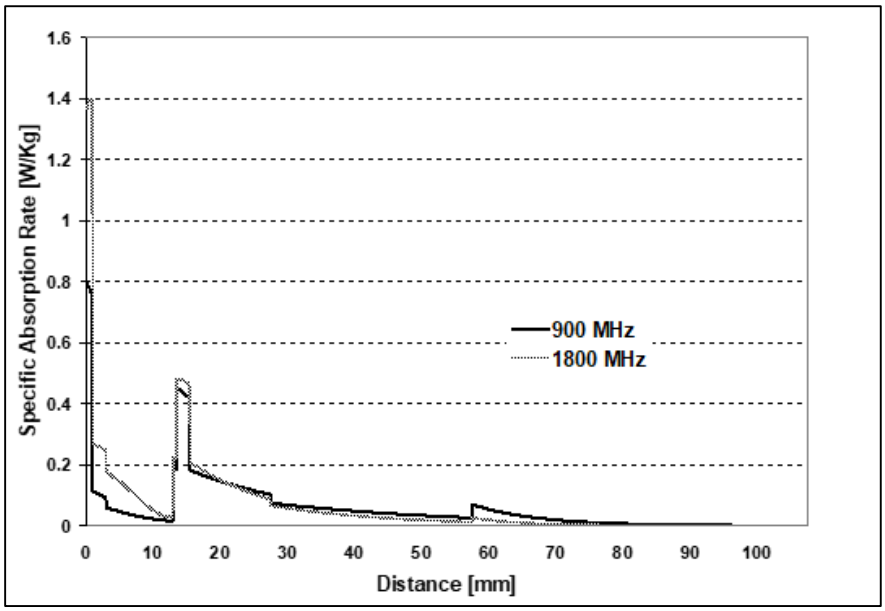

Figure 4 Local SAR distribution in elderly head

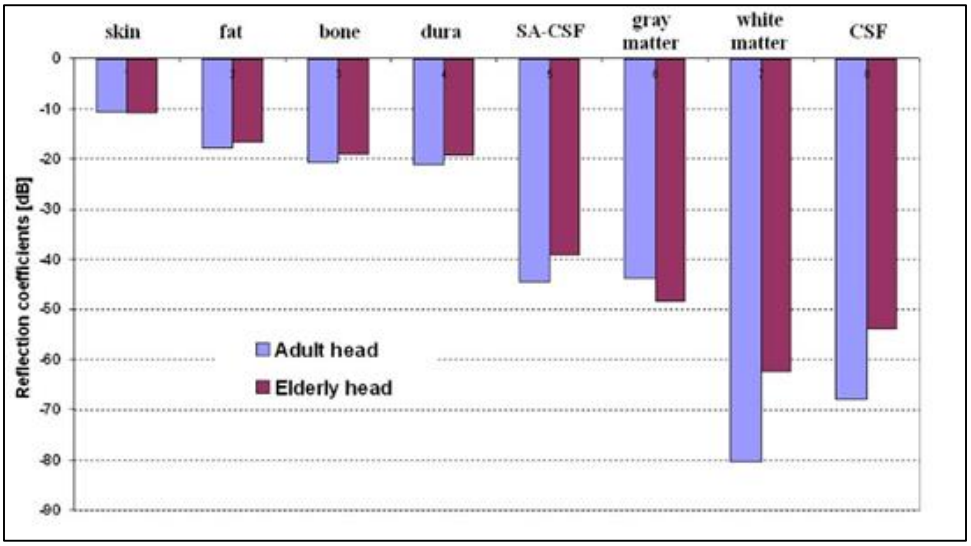

Figure 5 Magnitude of reflection coefficient for the different tissues in the model (20log|Γ|) at 900 MHz.

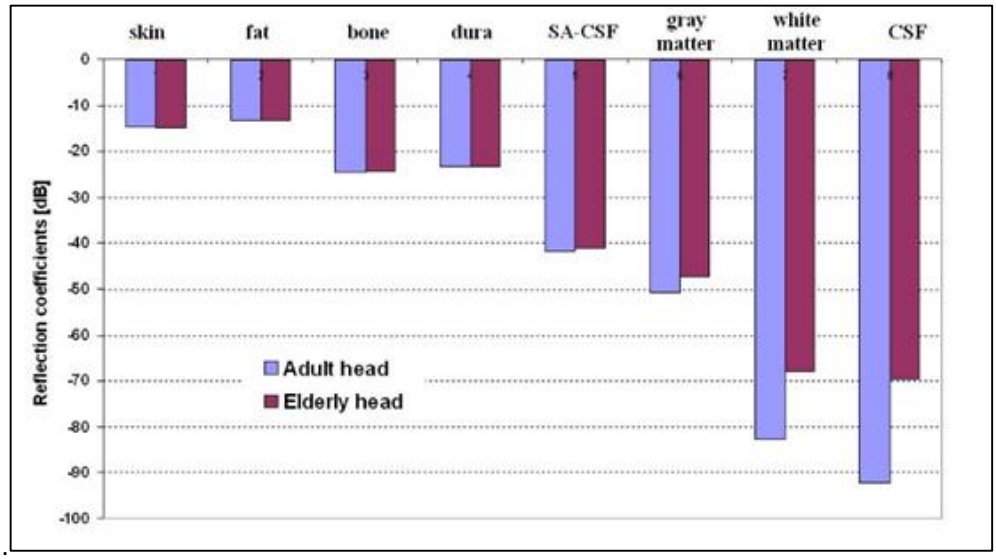

Figure 6 Magnitude of reflection coefficient for the different tissues in the model (20log|Γ|) at 1800 MHz.

The worst case tissue distributions for the maximum local SAR for an incident power of 1mW/cm^2 are given in Table 2.

Table 2 Maximum local SAR [W/Kg]

Tissue	**900 MHz**		**1800 MHz**	
	Adult	**Elderly**	**Adult**	**Elderly**
Skin	0.750	0.805	1.386	1.401
Fat	0.104	0.112	0.265	0.268
Bone	0.056	0.059	0.175	0.176
Dura	0.204	0.187	0.223	0.223
S – CSF	0.499	0.453	0.476	0.482

Graymatter	0.181	0.182	0.208	0.209
Whitematter	0.046	0.075	0.032	0.066
CSF	0.021	0.069	0.004	0.027

2.2. Two-dimensional (2-D) finite-difference time-domain (FDTD) formulation

One of the most successful and versatile methods for SAR calculations is the finite difference time domain (FDTD) method. The FDTD code with perfectly matched layer (PML) boundary conditions implemented according to the formulation proposed by Sullivan [17]. Following closely the theory in [17], the D_z field component in the finite difference formulation can be written as follows

$$\begin{aligned} D_z^{n+0.5}(i,j) &= gi3(i)gj3(j)D_z^{n-0.5}(i,j) \\ &+ 0.5gi2(i)gj2(j)* \\ &\left[\begin{array}{l} H_y^n(i+0.5,j) - H_y^n(i-0.5,j) \\ -H_x^n(i,j+0.5) + H_x^n(i,j-0.5) \end{array}\right] \end{aligned} \quad \text{.....(11)}$$

The parameters *gi2(i)* and *gi3(i)* (analogous to *gj2(j)* and *gj3(j),* respectively) are given by

$$\begin{aligned} gi2(i) &= 1/(1+xn(i)) \\ gi3(i) &= (1-xn(i))/(1+xn(i)) \end{aligned} \quad \text{..... (12)}$$

where *xn(i)* is given by

$$xn(i) = 0.333\left(i/No.of\ PML\ layers\right)^{3.0} \quad \text{..... (13)}$$
$$i = 1,2,\ldots, No.of\ PML\ layers$$

We can implement equation (11) in LabVIEW using two shift registers one to keep previous input value and the other to keep previous output values. Fig. 7 shows the implementation of D_z in the main FDTD loop.

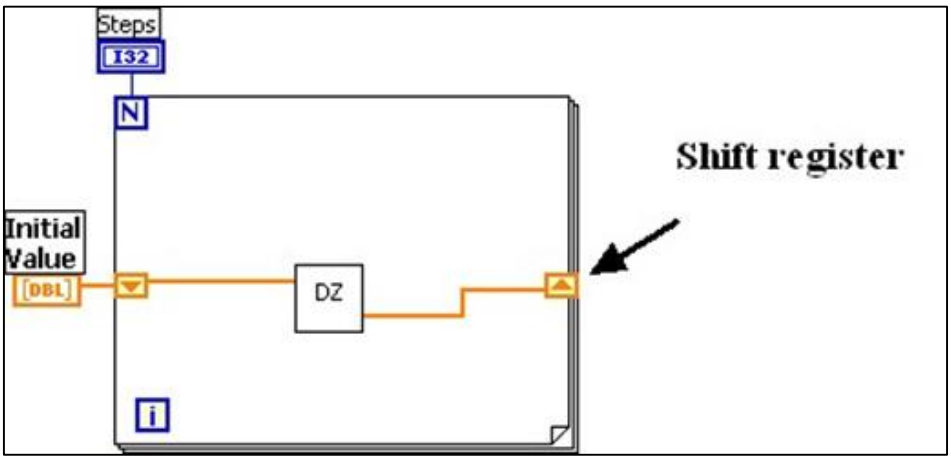

Figure 7 Update of the D_z field within main FDTD loop using shift registers

The above theory is applied to an eight-layered concentric cylindrical model of the human head. *l* denotes the number of layer. R_i is the radius of the ith boundary, where *i = 1,.., l* (Fig. 8). Table 3 shows the radii of the concentric cylindrical model (adult head). Free space is assumed for the outer space.

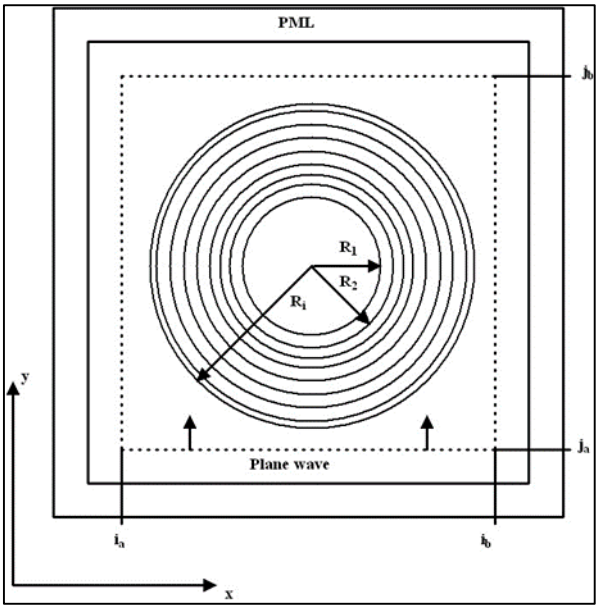

Figure 8 Update of the D_z field within main FDTD loop using shift registers.

A plane wave is used to excite *270* × *270* computational space. The problem space is divided into the total and scattered fields. A ten-cell air gap was used between the PML layer and the head model. The cell sizes were set as $\Delta x = \Delta y = 1.0$ *mm*. The simulations were run for *15* cycles.

Fig. 9 and 10 show the local SAR distributions at 900 and 1800 MHz for the two head models. The figures evidence the higher penetration depth at 900 MHz and the higher superficial SAR values at 1800 MHz. At the frequencies of 900 and 1800 MHz, SAR is higher for the elderly head model. However, at frequency of 900 MHz, SAR is decreased in few tissues of elderly head model namely, dura, S – CSF, gray matter and CSF.

It is worth noting that a greater amount of absorbed power occurs in the inner cylinders for 900 MHz rather than 1800 MHz.

Table 3 Radii of the concentric cylindrical model (normal adult head).

i	layer	Radius [cm]
1	CSF	1
2	White matter	6
3	Gray matter	8.2
4	S – CSF	8.4
5	Dura	8.45
6	Bone	9.45
7	Fat	9.65
8	Skin	9.75

Fig. 11 and Fig. 12 show the SAR distributions at the center of the concentric cylindrical model at 900 MHz and 1800 MHz for both models.

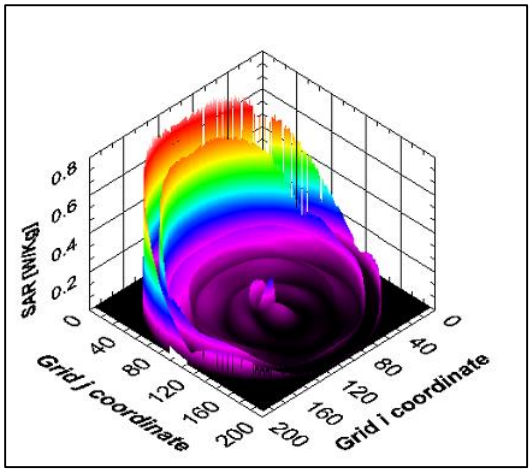

Figure 9(a) SAR distribution at 900 MHz for normal adult head model

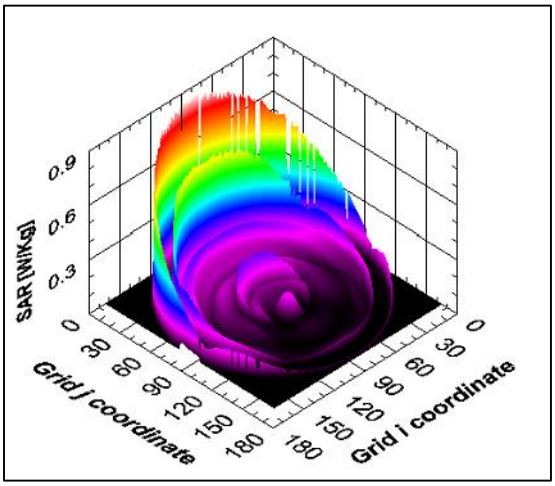

Figure 9(b) SAR distribution at 900 MHz for normal elderly head model.

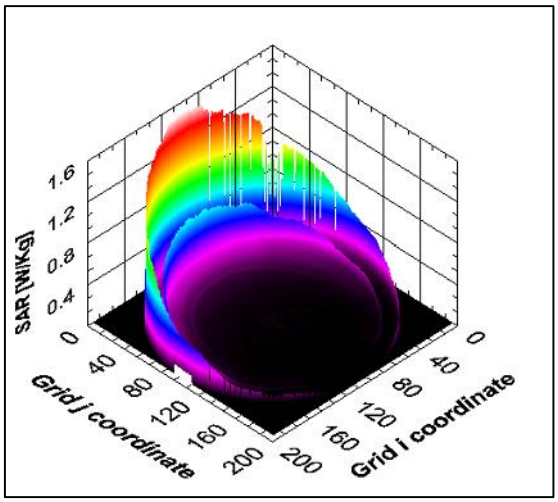

Figure 10(a) SAR distribution at 1800 MHz for normal adult head model

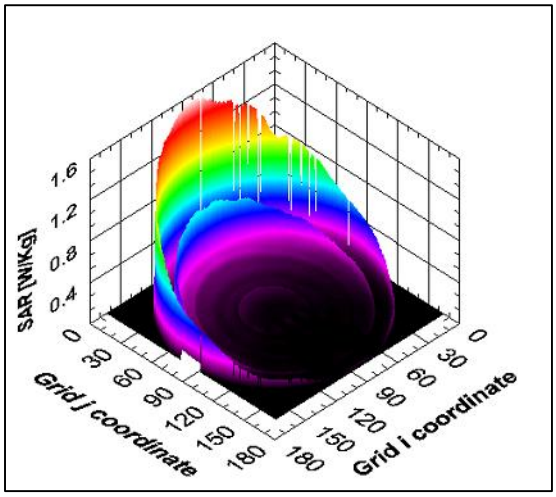

Figure 10(b) SAR distribution at 1800 MHz for normal elderly head model

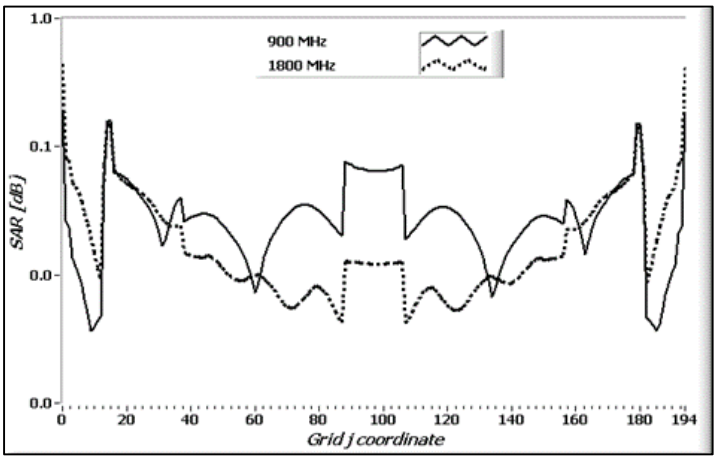

Figure 11 Normal adult head model

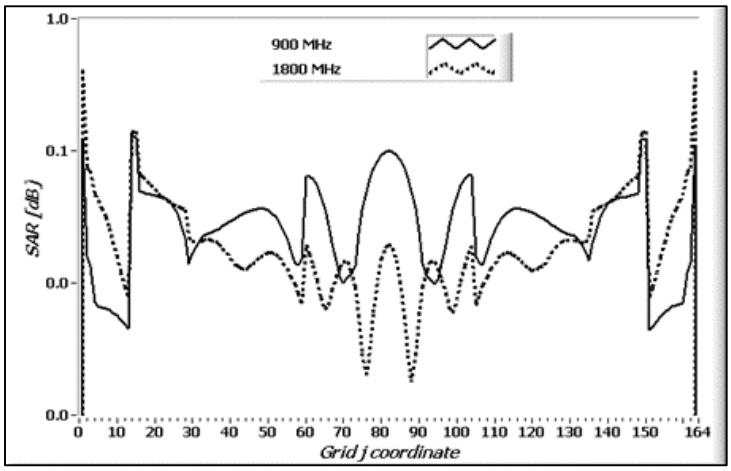

Figure 12 Normal elderly head model

3. Conclusion

The results presented in this paper constitute a unique and simplified approach to SAR estimation in the human head at 900 and 1800 MHz. It is apparent that significant differences do exist between the results for the adult head and elderly head models; the latter absorbs significantly more energy. However, since a greater amount of the absorbed power occurs in the inner cylinders for 900 MHz rather than 1800 MHz, the former constitutes a greater health hazard to elderly people at the same incident power.

It is also shown that the LabVIEW-based FDTD code is greatly extended FDTD range of applicability. In addition the code is relatively easily to understand and can be easily modified for the user's specific purpose.

References

[1] P. J. Dimbylow and O. P. Gandhi "Finite difference time domain calculations of SAR in a realistic heterogeneous model of the head for plane wave exposure from 600 MHz to 3 GHz," in *Phys. Med. Biol.,* 1991, 36(8), pp. 1075-1089.

[2] P. J. Dimbylow and S. M. Mann "SAR calculations in an anatomically realistic model of the head at 900 MHz and 1.9 GHz," in *Phys. Med. Biol.,* 1994, 39, pp. 1537-1553.

[3] M. A. Morgan, "Finite element calculation of microwave absorption by the cranial structure," in *IEEE Trans. Biomed. Eng.,* 1981, 28(10), pp. 687-695.

[4] A. Drossos and V. Santomaa and N. Kuster, "The dependence of electromagnetic energy absorption upon human head tissue composition in the frequency range o 300 – 3000 MHz," in *IEEE Trans. Microwave Theo. Tech.,* 2000, 48(11), pp. 1988-1995.

[5] *IEEE Standard for safety levels with respect to human exposure to radio frequency electromagnetic fields, 3 kHz to 300 GHz ,* ANSI/IEEE Standard C95.1-1992, 1992.

[6] International Commission on Non-Ionizing Radiation Protection, "*Health issues related to the use of hand-held radiotelephones and base transmittes,"* in *Health Phys.,* 1996, 70, pp. 587-593.

[7] AS Dekaban and D. Sadowsky, "Changes in brain weights during the span of human life: relation of brain weights to body heights and body weights," in *Annals of Neurology,* 1978, 4, pp. 354-356.

[8] N. C. Fox and J. M. Schott," Imaging cerebral atrophy: normal ageing to Alzheimer's disease," in *Lancet,* 2004, 363, pp. 392-394.

[9] A. Foundas and D. Zipin and C. Browning, "Age-realted changes of the insular cortex and lateral ventricles: conventional MRI volumetric measures," in *Journal of Neuroimaging,* 1998, 8, pp. 216-222.

[10] A. Gasmelseed and T. Andrew "A multi-layered model of human head irradiated by electromagnetic plane wave of 100 MHz – 300 GHz," in *Int. Journal of Sci. Res.,* 2006, 16, pp. 397-403.

[11] A. Taflove and M. Brodwin, "Numerical Solution of steady-state electromagnetic scattering problems using time-dependent Maxwell's equations," in *IEEE Trans. Microwave Theor. Tech.,* 1975, 23(8), pp. 623-630.

[12] A. Taflove, *Computational electrodynamics the finite difference time domain method,* Artech House Inc., Norwood, MA 1995.

[13] J. B. Olansen and E. Rosow, *Virtual bio-instrumentation, biomedical, clinical and healthcare applications in LabVIEW,* Virtual Instrumentation Series, National Instruments, 2001.

[14] R. Bitter and T. Mohiuddin and M. Nawrocki, *LabVIEW: advanced programming techniques,* CRC Press, 2000.

[15] J. Szentagothai, *Functional Anatomy,* Semmelweis Press, Budapest, 1994.

[16] C. Gabriel, *Compilation of the dielectric properties of body tissues at RF and microwave frequencies*, Radiofrequency Radiation Division, Brooks Air Force Base, Rep. N.AL/OE-TR-1996-0037, 1996.

[17] D. Sullivan, *Electromagnetic simulation using the FDTD method,* New York: IEEE Press, 2000.